

Determination of the contributions of degenerate and non-degenerate two-photon absorption response in silicon avalanche photodiode for infrared photon detection

Guangjian Xu , Xinyi Ren , Qucheng Miao , Ming Yan , Haifeng Pan , Xiuliang Chen , Guang Wu & E Wu

To cite this article: Guangjian Xu , Xinyi Ren , Qucheng Miao , Ming Yan , Haifeng Pan , Xiuliang Chen , Guang Wu & E Wu (2020): Determination of the contributions of degenerate and non-degenerate two-photon absorption response in silicon avalanche photodiode for infrared photon detection, Journal of Modern Optics, DOI: [10.1080/09500340.2020.1842926](https://doi.org/10.1080/09500340.2020.1842926)

To link to this article: <https://doi.org/10.1080/09500340.2020.1842926>



Published online: 19 Nov 2020.



Submit your article to this journal [↗](#)



Article views: 5



View related articles [↗](#)



View Crossmark data [↗](#)



Determination of the contributions of degenerate and non-degenerate two-photon absorption response in silicon avalanche photodiode for infrared photon detection

Guangjian Xu^a, Xinyi Ren^a, Qucheng Miao^a, Ming Yan^a, Haifeng Pan^a, Xiuliang Chen^a, Guang Wu^a and E Wu^{a,b}

^aState Key Laboratory of Precision Spectroscopy, East China Normal University, Shanghai, People's Republic of China; ^bCollaborative Innovation Center of Extreme Optics, Shanxi University, Taiyuan, People's Republic of China

ABSTRACT

The study of non-linear interactions in semiconductor photo-electronic devices to achieve effective and fast photon identification is an ongoing and important task. We investigated the specific contribution of degenerate and non-degenerate two-photon absorption (D-TPA and ND-TPA) response in silicon avalanche photodiode (Si-APD) for infrared photon detection at room temperature. We experimentally demonstrated that when the two laser pulses overlapped, the average D-TPA quantum detection efficiencies at 1800 nm, and that at 1550 nm were measured as 3.3×10^{-16} counts·pulse/photon², 4.3×10^{-15} counts·pulse/photon², respectively. And the ND-TPA quantum detection efficiency of 1800 nm and 1550 nm was measured to be 7.9×10^{-16} counts·pulse/photon². This study provides a solution for the practical infrared photon detection devices based on TPA effect in Si-APDs.

ARTICLE HISTORY

Received 26 April 2020
Accepted 21 October 2020

KEYWORDS

Degenerate and non-degenerate two-photon absorption; infrared photon detection; silicon avalanche photodiode

1. Introduction

Since the invention of the transistor more than half a century ago, semiconductor devices have been revolutionizing our daily lives, such as computers, smartphones, virtual reality devices and so forth. The photo-electronic devices such as photodetectors have become increasingly important by supporting various modern techniques. And recently, non-linear optical devices begin to develop vigorously to convert the infrared light to the visible regime or vice versa because the main information carrier in the optical cable network is in the infrared but detectors of infrared light is not as good as its counterpart for the visible regime [1,2]. Especially, in the fibre-based quantum cryptography where the information is encoded with single photons at the telecom wavelengths, the infrared single photon detectors played an extremely important role [3–6]. Different infrared single-photon detectors are developed including single-photon frequency upconversion detectors [7–9]. Moreover, non-linear optical devices based on high-order transitions between energy levels such as two-photon absorption (TPA) effect enables ultra-fast signal processing [10–12].

Non-linear optical equipment are commonly based on frequency-upconversion or TPA effect to achieve rapid infrared light signal processing and detection. The

frequency upconversion scheme is based on the sum-frequency generation process where the wavelength of the signal photons is transformed into the shorter wavelength region with the preservation of all the quantum characteristics and the upconverted photons finally impinge on the active area of a silicon-based detector for detection [13,14]. However, in the frequency upconversion system, special nonlinear crystals are designed and cut to fulfill the phase-matching conditions by adjusting the tilting angle and the operation temperature to maintain the momentum conservation for a high conversion efficiency [15–18]. At the same time, the TPA effect caused by the free electron in a semiconductor photodetector that absorbs two photons simultaneously, thereby achieving a transition from the ground state to the excited state and releasing a photoelectron by returning to the ground state can also be used for the detection of infrared photons [19,20]. For example, in a Si-avalanche photodiode (Si-APD) or other detector, the electron-hole pairs are created by TPA of the infrared photons and give rise to a photo-avalanche pulse output directly [21,22]. Infrared photon detection based on TPA effect has many advantages over the frequency upconversion scheme since the TPA effect is not constrained by the phase matching, and can provide a wide operating spectral range, making

the TPA scheme cheap and easy to integrate with other devices. In addition, the induced photocurrent of TPA is almost insensitive to the polarization state of the incident light.

In the TPA process, if the energies of the two absorbed photons are the same, it is the so-called the degenerate two-photon absorption (D-TPA), otherwise it is the so-called the non-degenerate two-photon absorption (ND-TPA). The TPA effect of semiconductors has been studied in different materials and structures. It has been experimentally demonstrated that the TPA effect can lead to an enhancement factor up to 100–1000 in direct-bandgap semiconductors [10]. The extremely ND-TPA in GaN photodiodes is utilized to perform scanned imaging of three-dimensional structures by infrared femtosecond laser pulse illumination [23]. The TPA effect in the commercial $\text{In}_{0.81}\text{Ga}_{0.19}\text{As}$ photodetector has been investigated to extend the nonlinear optical response to 4500 nm [24]. In addition, the nanostructured indium phosphide (InP) photodiode has been designed to detect the infrared light at room temperature using ND-TPA, and owing to the nanostructure, the photocurrent shows a gain of 24 with respect to the bulk response of InP [25]. The TPA effect has also been considered in silicon materials. For instance, a full band structure of TPA in bulk silicon has been theoretically calculated [26], and the D-TPA and Kerr coefficient of bulk Si for wavelength at 850 nm to 2200 nm has been measured in the experiment [27]. But the specific contribution value of D-TPA and ND-TPA effects in silicon photodetectors for infrared light detection has not been investigated so far as we known.

In this paper, we determined the contribution of D-TPA and ND-TPA effects for infrared light detection in the Si-APD single-photon detector at room temperature. When two beams of different wavelengths were casting on the active area of the detector with temporal separation, we got that the quantum detection efficiency of D-TPA at 1800 nm and 1550 nm was about 3.2×10^{-16} counts•pulse/photon² and 4.8×10^{-15} counts•pulse/photon², respectively. And when the two pulses coincided in time and space, the average quantum detection efficiency for the ND-TPA of 1800 and 1550 nm was measured as 7.9×10^{-16} counts•pulse/photon². This research has further broadened our understanding of the TPA effect in the silicon-based photo-electronics devices, and will promote the development of infrared photon detection via TPA in Si-APDs in extended applications.

2. Methods and experimental

In the experiment, we used an ultrabroadband fibre laser to study the D-TPA and ND-TPA induced photon

counting in the Si-APD. The experimental setup is sketched in Figure 1(a). The spectrum of the ultrabroadband fibre laser covered from 1200 nm to 1900 nm. The laser was passively mode-locked at a repetition rate of 55 MHz with a 10 ps pulse duration. The average output power was up to the mW level. A beam splitter was used to split the output laser into two beams. In one beam (Beam A), we used a germanium window to select the spectrum around 1800 nm as shown in Figure 1(b), while in the other beam (Beam B), a band-pass filter was inserted to select the spectrum around 1550 nm as shown in Figure 1(c). Two variable intensity attenuators were placed in each beam to adjust the incident photon fluxes. Then the two beams were combined by a dichroic mirror, and coupled into a fibre collimator by a lens. The photons from the combined beam were captured by a fibre-coupled single-photon detector based on Si-APD (SPCM-780-14-FC, Excelitas Tech.). The diameter of the active area of the Si-APD was about 180 μm . The photon flux incident to the Si-APD was evaluated according to the laser power and the transmittance loss of the two beams independently.

The photon-active area of the Si-APD functioned by the p-n junction of silicon, which band gap energy is 1.12 eV. According to the wavelengths of the two in beams in our experiment, we have

$$\hbar\omega_A, \hbar\omega_B < E_g < 2\hbar\omega_A, 2\hbar\omega_B, \quad (1)$$

where the E_g is the bandgap energy, ω_A and ω_B are the optical frequencies of Beam A and Beam B, respectively. Because both photon energies were lower than the band gap of silicon, it is impossible for the Si-APD to effectively respond those infrared photons over 1100 nm by the single-photon absorption. Therefore, the Si-APD has to absorb at least two photons to trigger a photo-induced avalanche output pulse, indicating the occurrence of the two- or three-photon absorption effects. But the efficiency of three-photon absorption is much smaller than that of the TPA. So we can attribute the detection of the infrared photons in Si-APD to the TPA effect alone. Since the two beams of different optical frequencies were incident on the Si-APD simultaneously, besides the D-TPA, the ND-TPA may also happen.

3. Result and discussion

In the semiconductor, the ND-TPA effect can be described according to the coupled-wave equation [28]

$$\frac{dI_1}{dz} = -2\alpha_2(\omega_1; \omega_2)I_1I_2, \quad (2)$$

$$\frac{dI_2}{dz} = -2\alpha_2(\omega_1; \omega_2)I_1I_2, \quad (3)$$

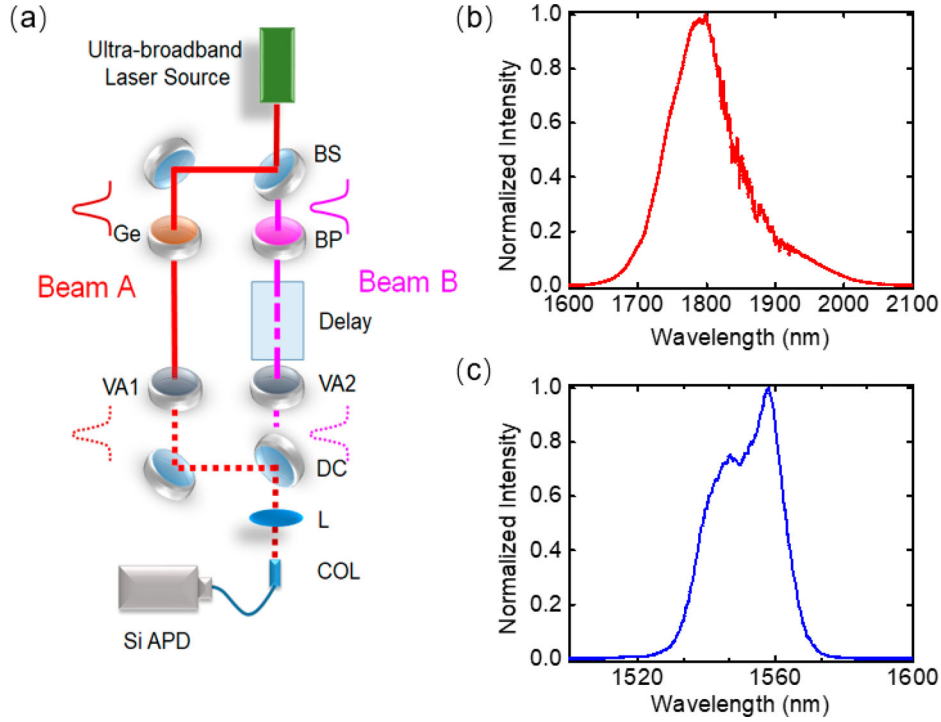


Figure 1. (a) Experimental setup. BS: Beamsplitter; Ge: Germanium window; BP: Bandpass filter at 1550 nm; VA1,2: Variable intensity attenuators; DC: Dichroic mirror reflecting 1800 nm and transmitting 1550 nm; L: Lens, COL: Fibre collimator; Si-APD: Single-photon detector based on silicon avalanche photodiode. Beam A is the beam around 1800 nm and Beam B is the beam around 1550 nm. (b) Spectrum of the Beam A at 1800 nm. (c) Spectrum of the Beam B at 1550 nm.

where I_1 and I_2 are the intensities of the incident light at the optical frequencies of ω_1 and ω_2 , respectively. And the TPA coefficient α_2 is governed by the scattering matrix formalism with two parabolic bands in Ref [28]

$$\alpha_2(\omega_1; \omega_2) = K \frac{\sqrt{E_p}}{n_1 n_2 E_g^3} F_2 \left(\frac{\hbar\omega_1}{E_g}; \frac{\hbar\omega_2}{E_g} \right), \quad (4)$$

where E_p is the Kane energy parameter, E_g is the bandgap energy, n_1, n_2 are the refractive indices of the material at ω_1 and ω_2 , respectively, and K is a material independent parameter. And the function F_2 is written as

$$F_2(x_1; x_2) = \frac{(x_1 + x_2 - 1)^{3/2}}{2^7 x_1 x_2^2} \left(\frac{1}{x_1} + \frac{1}{x_2} \right)^2. \quad (5)$$

Firstly, we studied the D-TPA in Si-APD, which means $\omega_1 = \omega_2$ in Equation (1). In the experiment, the two beams were incident on the Si-APD independently and we recorded the photon-counting rate as a function of the incident photon flux of Beam A and Beam B as shown in Figure 2. In a semiclassical approach, the photon counting rate of the Si-APD depends on the square of the incident photon flux as

$$C = \eta \langle N \rangle^2, \quad (6)$$

where η represents the quantum detection efficiency by the TPA effect and $\langle N \rangle$ is the photon flux of the incident light.

In D-TPA, the TPA response is a quadratic function of the incident light intensity. The slope of the logarithmic plots are 2.08 and 2.16 in Figure 2(a), and (b) respectively, which shows that the detector's response depends quadratically on the incident photon flux both at 1800 nm and 1550 nm. We can conclude that the Si-APD's response at these two wavelengths is dominated by the TPA effect. But note that in the measurement at 1800 nm, the incident photon flux ranges from 0.3×10^6 to 2.8×10^6 photons/pulse. Meanwhile, in the measurement at 1550 nm, the incident photon flux ranges from 0.06×10^6 to 0.7×10^6 photons/pulse. The photon counting rates were at the same level. The big difference is caused by the TPA coefficient α_2 of the Si-APD at the two wavelengths.

Then, we tuned the VAs to adjust the photon counting rate of Beam A and B at about 135 kHz and 125 kHz, respectively. Both beams were injected to the detector but the pulse trains from the two were with a temporal delay much longer than the laser pulse duration. As shown in Figure 3, the two endpoints of the total photon counting rate represented by the blue triangles are the same as the sum from the two beams by the purple inverted

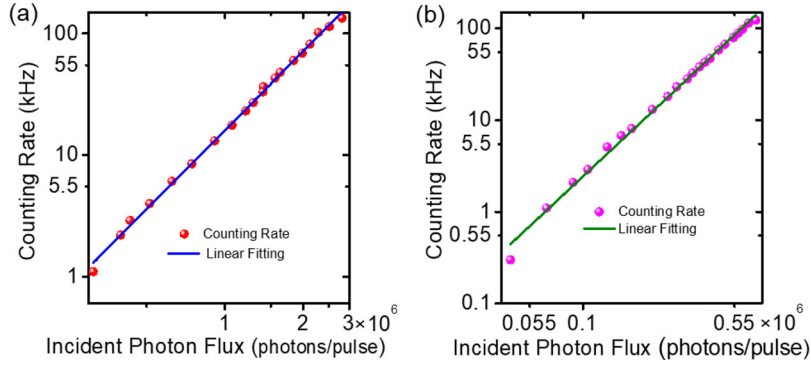


Figure 2. Photon-counting rate as a function of the incident photon flux with a single beam at 1800 nm (a) and 1550 nm (b), respectively.

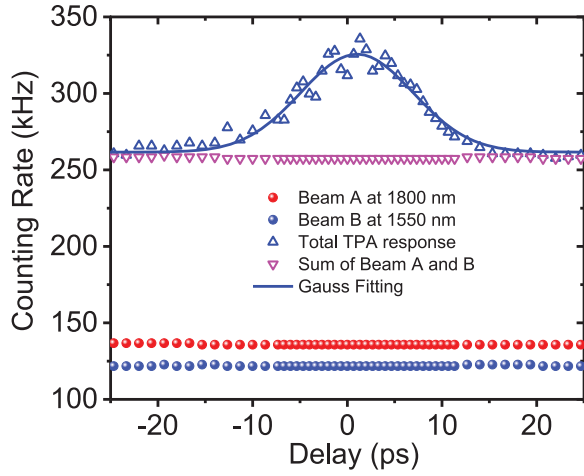


Figure 3. Photon counting rate as a function of the relative delay between the two beams. The bottom two lines made of spots are the counting rate of the D-TPA of 1800 nm (upper) and 1550 nm (lower) respectively. The pink triangle spots are the sum of the both D-TPA effect. And the blue triangle spots are the counting rate of the TPA of two beams.

triangles, showing that the Si-APD's response was from the TPA of each beam if the two pulses did not overlap each other. The photon counting rate is about 260 kHz, which was almost the same as the sum of that from the two beams. Tuning the time delay between the two beams, the total counting rate of the Si-APD increased and reached a maximum when the two beams were temporally overlapped. This increase in the photon counting rate was considerably caused by the ND-TPA. Similar to the principle of an optical autocorrelator, when the phase difference between the two beams was zero, ND-TPA got a maximum of 325 kHz. The full-width at half maximum of the curve is 14.2 ps, in good agreement with the laser pulse duration of 10 ps with $t = \sqrt{2}\tau$, where t is the measured cross-correlation width and τ is the laser pulse duration.

Fixing the delay at zero, we could study the ND-TPA by comparing with D-TPA. We adjusted the incident

photon fluxes of both beams to keep the photon counting rate at a certain value. In this case, the response of the Si-APD included both the ND-TPA contributed by the two beams and also the D-TPA from each beam individually. The photon counting rate follows

$$C = \eta_{AB}\langle N_A \rangle \langle N_B \rangle + \eta_A \langle N_A \rangle^2 + \eta_B \langle N_B \rangle^2, \quad (7)$$

where $\eta_{AB}\eta_A\eta_B$ represent the quantum detection efficiency by the ND-TPA effect, D-TPA of Beam A, and D-TPA of Beam B respectively. And $\langle N_A \rangle$ and $\langle N_B \rangle$ are the photon fluxes of Beam A and Beam B, respectively. We adjusted the incident photon fluxes by the two VAs while keeping a certain total photon counting rate ranging from 27 kHz to 160 kHz as shown in Figure 4(a). By fitting the curves in Figure 4(a) according to Equation (7), we get

$$\begin{aligned} \eta_{AB} &= (7.9 \pm 1.5) \times 10^{-16} \text{ counts} \cdot \text{pulse}/\text{photon}^2, \\ \eta_A &= (3.3 \pm 0.1) \times 10^{-16} \text{ counts} \cdot \text{pulse}/\text{photon}^2, \\ \eta_B &= (4.3 \pm 0.26) \times 10^{-15} \text{ counts} \cdot \text{pulse}/\text{photon}^2. \end{aligned} \quad (8)$$

Meanwhile, the D-TPA quantum detection efficiency were determined by recording the photon counting rates when the delay between the two beams was far from zero. The incident photon fluxes were recorded in the same way as in the ND-TPA measurement. All the curves are in a quarter ellipse shape obeying

$$C' = \eta_A \langle N_A \rangle^2 + \eta_B \langle N_B \rangle^2. \quad (9)$$

And by fitting the curves in Figure 4(b), we get

$$\begin{aligned} \eta_A &= (3.2 \pm 0.2) \times 10^{-16} \text{ counts} \cdot \text{pulse}/\text{photon}^2, \\ \eta_B &= (4.8 \pm 0.12) \times 10^{-15} \text{ counts} \cdot \text{pulse}/\text{photon}^2, \end{aligned} \quad (10)$$

which are almost the same as those in Equation (8). We can conclude that the quantum detection efficiency of D-TPA keeps the same in the presence of ND-TPA.

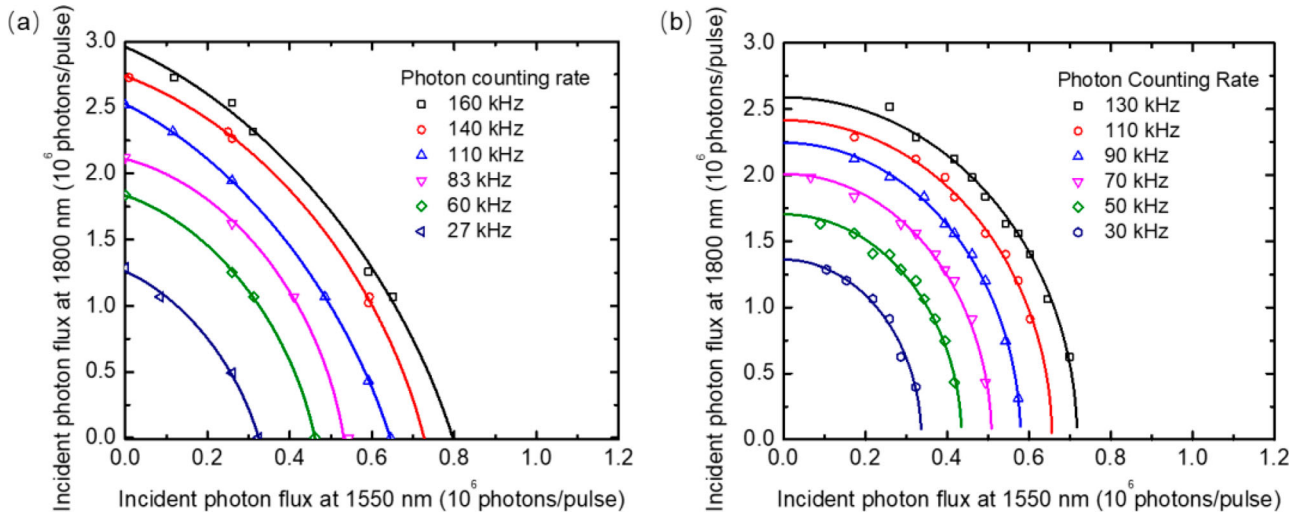


Figure 4. Incident photon flux of two beams at a certain counting rate under total TPA effect (a) and D-TPA effect alone (b).

The spectral dependence of the TPA efficiency is expected to be different for indirect gap semiconductor as compared with that of the direct-gap semiconductors. According to Ref [29], the D-TPA coefficient has a maximum slightly above the indirect bandgap, at $\hbar\omega \cong (7/6)E_g$. Accordingly, the wavelength of the photon is at about 954 nm. As the wavelength increases, the D-TPA efficiency decreases [27]. The D-TPA quantum detection efficiency at 1800 nm was measured to be more than one order smaller than that at 1550 nm in our experiment. Meanwhile, the ND-TPA efficiency was not equal to the D-TPA efficiency at either wavelength of 1800 nm and 1550 nm. And there was no direct relation between the ND-TPA efficiency and the D-TPA efficiencies of the two beams at different wavelengths. In this ND-TPA process, we can consider one of the beam as the pump and the other beam as the signal. Therefore, when the pump laser at 1550 nm reached 8.35 mW (peak power), we obtained the quantum detection efficiency of Si-APD at 1800 nm as 7.9×10^{-10} . Accordingly, if we used the laser beam at 1800 nm as the pump, the quantum detection efficiency of Si-APD due to ND-TPA at 1550 nm was 3.03×10^{-9} when the pump laser power was 34.96 mW (peak power). The detection efficiency based on the ND-TPA is much lower than that of the InGaAs avalanche photodiode or the superconducting nanowire detectors, but it provides us alternate solution for the infrared photon detection.

4. Conclusion

In summary, we experimentally determined the specific contribution of D-TPA and ND-TPA effects at two different wavelengths of 1800 nm and 1550 nm for infrared light detection in the Si-APD single-photon detector

at room temperature. The quantum detection efficiencies of D-TPA at 1800 nm and 1550 nm were measured to be about 3.2×10^{-16} counts \cdot pulse/photon² and 4.8×10^{-15} counts \cdot pulse/photon², respectively, and they kept the same in the presence of ND-TPA. Meanwhile the quantum detection efficiency of ND-TPA of 1550 nm and 1800 nm was measured to be 7.9×10^{-16} counts \cdot pulse/photon². The TPA effect in photon detectors has shown great potential in many applications. Owing to the advantages of infrared photon detection based on TPA effect over the frequency upconversion scheme, we believe that high efficiency TPA quantum detectors of silicon-based optoelectronic devices will be developed in the near future for various applications.

Acknowledgements

We thank Professor Kun Huang from East China Normal University for discussions.

Disclosure statement

No potential conflict of interest was reported by the author(s).

Funding

This work was supported by National Key R&D Program (2018YFB0504400); National Natural Science Foundation of China [grant numbers 11722431, 11774095, 11621404].

Availability of data and materials

The datasets used and/or analyzed during the current study are available from the corresponding author on reasonable request.

References

- [1] Rakher MT, Ma L, Slattery O, et al. Quantum transduction of telecommunications-band single photons from a quantum dot by frequency upconversion. *Nat Photon.* **2010**;4:786–791.
- [2] Kuzucu O, Wong FNC, Kurimura S, et al. Joint temporal density measurements for two-photon state characterization. *Phys Rev Lett.* **2008**;101:153602.
- [3] Wang S, He D, Yin Z, et al. Beating the fundamental rate-distance limit in a proof-of-principle quantum key distribution system. *Phys Rev X.* **2019**;9:021046.
- [4] Qian Y, He D, Wang S, et al. Robust countermeasure against detector control attack in practical quantum key distribution system. *Optica.* **2019**;6:1178–1184.
- [5] Yin Z, Wang S, Chen W, et al. Improved security bound for the round-robin-differential-phase-shift quantum key distribution. *Nat Commun.* **2018**;9:457.
- [6] He D, Wang S, Chen W, et al. Sine-wave gating InGaAs/InP single photon detector with ultralow afterpulse. *Appl Phys Lett.* **2017**;110:111104.
- [7] Liao S, Yong H, Liu C, et al. Long-distance free-space quantum key distribution in daylight towards inter-satellite communication. *Nat Photon.* **2017**;11:509–513.
- [8] Iwal Y, Honjo T, Inoue K, et al. Polarization-independent, differential-phase-shift, quantum-key distribution system using upconversion detectors. *Opt Lett.* **2009**;34:1606–1608.
- [9] Namekata N, Makino Y, Inoue S. Single-photon detector for long-distance fiber-optic quantum key distribution. *Opt Lett.* **2002**;27:954–956.
- [10] Fishman DA, Cirloganu CM, Webster S, et al. Sensitive mid-infrared detection in wide-bandgap semiconductors using extreme non-degenerate two-photon absorption. *Nat Photon.* **2011**;5:561–565.
- [11] Apiratikul P, Murphy TE. Background-suppressed ultrafast optical sampling using nondegenerate two-photon absorption in a GaAs photodiode. *IEEE Photon Technol Lett.* **2010**;22:212–214.
- [12] Maguire PJ, Barry LP, Krug T, et al. Optical signal processing via two-photon absorption in a semiconductor microcavity for the next generation of high-speed optical communications network. *J Lightw Technol.* **2006**;24:2683–2692.
- [13] Gomes JT, Delage L, Baudoin R, et al. Laboratory demonstration of spatial-coherence analysis of a blackbody through an up-conversion interferometer. *Phys Rev Lett.* **2014**;112:143904.
- [14] Tang R, Li X, Wu W, et al. High efficiency frequency upconversion of photons carrying orbital angular momentum for a quantum information interface. *Opt Express.* **2015**;23(8):9796–9802.
- [15] Barh A, Pedersen C, Tidemand-Lichtenberg P. Ultra-broadband mid-wave-IR upconversion detection. *Opt Lett.* **2017**;42:1504–1507.
- [16] Gu X, Huang K, Li Y, et al. Temporal and spectral control of single-photon frequency upconversion for pulsed radiation. *Appl Phys Lett.* **2010**;96:131111.
- [17] Meng L, Padye A, Pedersen C, et al. SHG (532 nm)-induced spontaneous parametric downconversion noise in 1064-nm-pumped IR upconversion detectors. *Opt Lett.* **2019**;44:1670–1673.
- [18] Ma J, Chen X, Hu H, et al. Quantum detector tomography of a single-photon frequency upconversion detection system. *Opt Express.* **2016**;24:20973–20981.
- [19] Olszak PD, Cirloganu CM, Webster S, et al. Spectral and temperature dependence of two-photon and free-carrier absorption in InSb. *Phys Rev B.* **2010**;82:235207.
- [20] Boiko DL, Antonov AV, Kuritsyn DI, et al. Mid-infrared two photon absorption sensitivity of commercial detectors. *Appl Phys Lett.* **2017**;111:171102.
- [21] Hayat A, Ginzburg P, Orenstein M. Infrared single-photon detection by two-photon absorption in silicon. *Phys Rev B.* **2008**;77:125219.
- [22] Xu G, Ren X, Miao Q, et al. Sensitive infrared photon counting detection by nondegenerate two-photon absorption in Si APD. *IEEE Photon Tech Lett.* **2019**;31:1944–1947.
- [23] Pattanaik HS, Reichert M, Hagan DJ, et al. Three-dimensional IR imaging with uncooled GaN photodiodes using nondegenerate two-photon absorption. *Opt Express.* **2016**;24:1196.
- [24] Piccardo M, Rubin NA, Meadowcroft L, et al. Mid-infrared two-photon absorption in an extended-wavelength InGaAs photodetector. *Appl Phys Lett.* **2018**;112(4):041106.
- [25] Fix B, Jaeck J, Vest B, et al. Nanostructured diode for infrared photodetection through nondegenerate two-photon absorption. *Appl Phys Lett.* **2017**;111(4):041102.
- [26] Cheng JL, Rioux J, Sipe JE. Full band structure calculation of two-photon indirect absorption in bulk silicon. *Appl Phys Lett.* **2011**;98(13):131101.
- [27] Bristow AD, Rotenberg N, Van Driel HM. Two-photon absorption and Kerr coefficients of silicon for 850–2200 nm. *Appl Phys Lett.* **2007**;90(19):191104.
- [28] Sheik-Bahae M, Hutchings DC, Hagan DJ, et al. Dispersion of bound electronic nonlinear refraction in solids. *IEEE J Quant Electr.* **1991**;27(6):1296–1309.
- [29] Dinu M. Dispersion of phonon-assisted nonresonant third-order nonlinearities. *IEEE J. Quant Electr.* **2003**;39(11):1498–1503.